Physica A 389 (2010) 5662–5670

Contents lists available at ScienceDirect

Physica A

journal homepage: www.elsevier.com/locate/physa

Monofractal and multifractal analysis of simulated heat release fluctuations in a spark ignition heat engine

P.L. Curto-Risso [a,1], A. Medina [b,2], A. Calvo Hernández [b], L. Guzmán-Vargas [c,*], F. Angulo-Brown [d]

[a] Departamento de Física Aplicada - IIMPI, Universidad de República, Montevideo, Uruguay

[b] Departamento de Física Aplicada, Universidad de Salamanca, 37008 Salamanca, Spain

[c] Unidad Profesional Interdisciplinaria en Ingeniería y Tecnologías Avanzadas, Instituto Politécnico Nacional, Av. IPN No. 2580, L. Ticomán, México D.F. 07340, Mexico

[d] Departamento de Física, Escuela Superior de Física y Matemáticas, Instituto Politécnico Nacional, Edif. No. 9 U.P. Zacatenco, México D.F. 07738, Mexico

ARTICLE INFO

Article history:
Received 7 June 2010
Received in revised form 30 July 2010
Available online 15 September 2010

Keywords:
Cyclic variability
Fractal
Heat engine

ABSTRACT

We study data from cycle-by-cycle variations in heat release for a simulated spark-ignited engine. Our analyses are based on nonlinear scaling properties of heat release fluctuations obtained from a turbulent combustion model. We apply monofractal and multifractal methods to characterize the fluctuations for several fuel–air ratio values, ϕ, from lean mixtures to stoichiometric situations. The monofractal approach reveals that, for lean and stoichiometric conditions, the fluctuations are characterized by the presence of weak anticorrelations, whereas for intermediate mixtures we observe complex dynamics characterized by a crossover in the scaling exponents: for short scales, the variations display positive correlations while for large scales the fluctuations are close to white noise. Moreover, a broad multifractal spectrum is observed for intermediate fuel ratio values, while for low and high ϕ the fluctuations lead to a narrow spectrum. Finally, we explore the origin of correlations by using the surrogate data method to compare the findings of multifractality and scaling exponents between original simulated and randomized data.

1. Introduction

In general, typical thermodynamic models of thermal cycles are focused on operating in steady-state conditions, and only one cycle is taken as representative of all other cycles pertaining to a sequence of the latter [1]. For example, in a typical internal combustion engine, several thousands of cycles can be performed in a minute, and there exist experimental and theoretical reasons to expect significant variations from one cycle to the next. Those variations can be found for example in the combustion heat and maximum pressure of spark-ignition engines [2–5]. Many thermal and mechanical phenomena support the so-called cyclic variability (CV), which is concomitant with a very complex dynamical behavior. In fact, in recent years, many researchers have investigated CV by means of nonlinear dynamics methods and chaos theory [2–6].

Although CV phenomena have been observed since the 19th century, nowadays there exists a debate about the true nature of CV [2,4]. Among the physical causes of CV [7,8], the motion of the gas mixture and the turbulences throughout

* Corresponding author.
E-mail addresses: pcurto@fing.edu.uy (P.L. Curto-Risso), amd385@usal.es (A. Medina), anca@usal.es (A. Calvo Hernández), lguzmanv@ipn.mx (L. Guzmán-Vargas), angulo@esfm.ipn.mx (F. Angulo-Brown).

1 Also at Instituto de Ingeniería Mecánica y Producción Industrial, Universidad de la República Oriental del Uruguay.

2 Also at ETSII de Béjar, Universidad de Salamanca, 37700 Béjar, Salamanca, Spain.

0378-4371/$ – see front matter © 2010 Elsevier B.V. All rights reserved.
doi:10.1016/j.physa.2010.08.024

combustion are the most important. During admission and exhaust processes, valves are simultaneously open (overlapping period), so not all the burned gases are expelled, and variations of the chemical composition of the mixture (fuel, air and residual gases) in each cycle thus influences the heat release during combustion. Other factors that could influence the cycle-by-cycle variations are the homogeneity of the mixture composition, especially in the vicinity of the spark plug, as well as details of the spark discharge (breakdown energy, initial flame kernel position). Of course, fluctuations of the thermodynamic cycle developed by the engine provoke significant changes in performance records such as power output and efficiency [9].

In analyzing these kinds of fluctuation, many authors have reported extensive work by looking at different variables such as maximum pressures or heat release by means of different statistical methods such as return maps [10], recurrence plots, correlation coarse-grained entropy [11,10], and sample entropy [10]. Daw et al. [2] proposed a discrete engine model that explains how both stochastic and deterministic features can be observed in a spark-ignited internal combustion engine, and they reproduced experimental observations.

Recently, Sen et al. [5,4] investigated the complex dynamics of experimental cycle-to-cycle heat release variations in a spark-ignition engine by using multifractal methods. The monofractal and multifractal properties of irregular and nonstationary signals can be described with global and local invariant quantities. Multifractal structures have been found in a growing number of complex systems, such as physiological time series, geophysics data records, and financial indicators [12–19]. Many of the nonlinear statistical analyses of spark-ignition engine dynamical behavior have been carried out on experimental data, while others have been made using theoretical models and computer simulations.

This work is located within computer simulations studies, and a main goal is to analyze the effect of some combustion parameters and their consequences on CV for fuel–air equivalence ratios ranging from lean mixtures to stoichiometric conditions, by using both monofractal and multifractal methods. To do this, we use a quasi-dimensional computer simulation that includes turbulent combustion, valves overlapping, heat transfer across the cylinder walls, and a detailed analysis of the chemical reaction involved. This simulation was previously validated and it reproduces the main characteristics of heat release fluctuant time series [20,21]. The monofractal method used is the Higuchi fractal dimension [22], and the multifractal one we follow is the wavelet multifractal method [12].

The paper is organized in the following way. Section 2 is devoted to briefly describing the basic elements of our quasi-dimensional computer simulation with special emphasis on combustion [23,20,21]. In Section 3, we briefly describe the monofractal and multifractal methods. In Section 4, we analyze the simulation results for heat release time series at different values of the fuel/air equivalence ratio. Finally, in Section 5, we discuss our results and summarize the main conclusions of the paper.

2. Simulated model

We previously developed a quasi-dimensional computer simulation of a monocylindrical Otto engine, which was validated in [20]. The model also reproduced the main features of cyclic variability when compared with experiments such as the evolution with the fuel ratio of the statistical parameters characterizing heat release time series and the corresponding return maps [21].

Quasi-dimensional models solve explicit differential equations for the evolution of burned and unburned masses of the fuel–air mixture during combustion, considering that the flame front is approximately spherical. In the model considered, two ordinary differential equations are solved for each time step or crankshaft angle for the pressure and the temperature of the gases inside the cylinder during all steps of the engine evolution. In particular, in combustion (the most important process in cycle-by-cycle variations) we consider a two-zone model, discerning between unburned (u) and burned (b) gases separated by an adiabatic flame front with negligible volume. We assume the turbulent eddy-burning or entrainment model proposed by Keck [24,25] and Beretta [26].

The model considers that during flame propagation not all the mass within the flame front is burned, but there exist unburned eddies of typical length l_t. The coupled system of equations for the masses of the burned gas mixture m_b and the total mass within the flame front m_e (unburned eddies plus burned gas) reads as follows:

$$\dot{m}_b = \rho_u A_f S_l + \frac{m_e - m_b}{\tau_b}, \tag{1}$$

$$\dot{m}_e = \rho_u A_f \left[u_t \left(1 - e^{t/\tau_b}\right) + S_l\right], \tag{2}$$

where u_t is the characteristic velocity at which unburned gases pass through the flame front, ρ_u is the unburned gas density, and A_f is the flame front area. $\tau_b = l_t/S_l$ is the characteristic time for the combustion of the entrained eddies and S_l is the laminar combustion speed, which is determined from its value at reference pressure and temperature conditions [27–29]. Laminar speeds obviously depend on the thermodynamic conditions but also on the fuel/air equivalence ratio and on the mole fraction of gases in the chamber after combustion. In other words, S_l connects the combustion dynamics and the proportion of residual gases in the cylinder after the previous event, the memory of the chemistry of combustion. Together with gas mixture motion, turbulences during combustion and the homogeneity of the mixture composition near the spark plug, memory effects are considered by several authors as the main physical ingredients of cyclic variability [7,8].

Among the parameters that determine the development of combustion, there are three essential ones: the characteristic length of eddies l_t (associated to the characteristic time, τ_b), the turbulent entrainment velocity u_t (essential for the slope of

$m_e(t)$ during the fastest stage of combustion), and the location of the ignition kernel that gives the size and geometry of the flame front. Therefore, all these parameters could have strong influence on cycle-by-cycle variations. A recent study [21] has shown that the incorporation of stochastic fluctuations at least on l_t or u_t is essential to reproduce the main characteristics of heat release fluctuations that appear in experimental results.

The chemistry and the energetics of combustion were solved by means of the routine developed by Ferguson [30] (but including residual gases among the reactants). Thus, the unburned gas mixture is formed by a standard fuel for spark ignition engines (iso-octane, C_8H_{18}), air, and exhaust gases. Our model does not consider traces of C_8H_{18} in the combustion products, but the energy release includes combustible elements such as CO, H, or H_2. The thermodynamic properties of all the chemical species involved are obtained from the constant pressure specific heats, which are taken as 7-parameter temperature polynomials [31].

Heat release during combustion is numerically evaluated through the first principle of thermodynamics for open systems, separating the heat release, δQ_r, internal energy variations associated to temperature changes, dU, net work output (excluding friction losses), δW, and heat transfers from the working fluid (considered as a mixture of ideal gases) to the cylinder walls, δQ_ℓ:

$$\delta Q_r = dU + \delta W + \delta Q_\ell, \tag{3}$$

where the internal energy and heat losses include terms associated to either unburned or burned gases. Woschni's model [32,33] was followed to account for heat losses through cylinder walls, Q_ℓ, and work losses due to piston frictions were quantified as in [20,23]. All these terms can be derived in terms of time or of the crankshaft angle. The net heat release during the whole combustion period is calculated from the integration of heat release variation during that period.

As a summary of this theoretical section, it is important to note that in our dynamical system the coupled ordinary differential equations for pressure and temperature are in turn coupled with two other ordinary differential equations for the evolution of the masses during combustion. All these variables evolve with time or with the crankshaft angle. As recently shown, this deterministic scheme does not reproduce the experimental characteristics showed by heat release fluctuations. The incorporation of stochastic fluctuations on the characteristic length of unburned eddies during combustion, l_t, or on the characteristic velocity at which unburned gases pass through the flame front, u_t, allows us to reproduce the main features of heat release time series and their evolution with fuel/air equivalence ratio [20,23,33].

3. Methods

3.1. Fractal dimension method

The power spectrum is the typical method used to characterize auto-correlations in time series. For example, consider a stationary stochastic process with an autocorrelation function which follows a power law $C(s) \sim s^{-\gamma}$, where s is the lag and γ is the correlation exponent, $0 < \gamma < 1$. The presence of long-term correlations is related to the fact that the mean correlation time diverges for infinite time series. According to the Wiener–Khintchin theorem, the power spectrum is the Fourier transform of the autocorrelation function $C(s)$, and for the case described above, we have the scaling relation $S(f) \sim f^{-\beta}$, where β is called the spectral exponent and it is related to the correlation exponent by $\gamma = 1 - \beta$. Alternative methods have been proposed for the assessment of correlations and fractal properties for stationary and nonstationary time series [34–36]. In [22], Higuchi proposed a method to calculate the fractal dimension (the fractal dimension method, FDM) of self-affine curves in terms of the slope of the straight line that fits the length of the curve versus the time interval (the lag) in a double log plot. The method consists in considering a finite set of data taken at an interval $\nu_1, \nu_2, \ldots, \nu_N$. From this series, we construct new time series, v_m^k, defined as

$$\nu(m), \nu(m+k), \nu(m+2k), \ldots, \nu\left(m + \left[\frac{N-k}{k}\right] \cdot k\right); \quad \text{with } m = 1, 2, 3, \ldots, k, \tag{4}$$

where [ ] denotes Gauss' notation, that is, the bigger integer, and m and k are integers that indicate the initial time and the interval time, respectively. The length of the curve v_m^k, is defined as

$$L_m(k) = \frac{1}{k}\left[\left(\sum_{i=1}^{\left[\frac{N-m}{k}\right]} |\nu(m+ik) - \nu(m+(i-1)k)|\right)\frac{N-1}{\left[\frac{N-m}{k}\right]k}\right] \tag{5}$$

and the term $(N-1)/[(N-m)/k]k$ represents a normalization factor. Then, the length of the curve for the time interval k is given by $\langle L(k)\rangle$: the average value over k sets $L_m(k)$. Finally, if $\langle L(k)\rangle \propto k^{-D}$, then the curve is fractal, with dimension D [22]. The fractal dimension is related to the spectral exponent β by means of $\beta = 5 - 2D$ [22]. Note that this relationship is valid for $1 < D < 2$ and $1 < \beta < 3$. For an uncorrelated random walk, which results from the integration of white noise fluctuations, we observe that $D = 1.5$. For β within the interval $-1 < \beta < 1$, that is, for processes which can be described as the first derivative of fluctuations with spectral exponent within the interval $1 < \beta < 3$, the relationship between β and D changes to $\beta = 3 - 2D$. A process with positive long-range correlations leads to $D < 1.5$, whereas for anticorrelated processes $D > 1.5$.

3.2. Multifractal method

In many cases, fluctuations from physical and biological systems exhibit a complex behavior which is not fully characterized by a single scaling exponent. For this type of system, a larger number of exponents is necessary to characterize their scaling properties. Multifractal signals can be analyzed at many scales with different local scaling exponents (Hurst exponents, h). The local Hurst exponent quantifies the singular behavior for a given scale. For monofractal signals, the local exponent is the same for the entire signal ($h = H$), with H the global Hurst exponent. It is known that for positively correlated signals the value of the H exponent ranges from 1/2 to 1 ($1/2 < H < 1$), whereas for anticorrelated processes $0 < H < 1/2$. In fact, for monofractal signals there is a relationship between H and the fractal dimension of the time series D, given by $D = 2 - H$ [37,38]. Time series with multifractal properties are characterized by a set of local exponents h which conform to the function $f(h)$, where $f(h)$ represents the fractal dimension of the subset of the signal characterized by the local exponent h. To determine the values of the local exponents h, we apply the wavelet multifractal method (WMM), which is very suitable for the analysis of multifractal signals [39,12,40]. The wavelet transform is very appropriate, because it can remove local trends, reducing the effects of nonstationarities. Specifically, we use the wavelet transform modulus maxima method to calculate h. The third derivative of the Gaussian function was used as the wavelet function in all our calculations [39,12]. First, we consider a partition function $Z_q(a)$ defined as the sum of the qth powers of the local maxima of the modulus of the wavelet transform coefficient at scale a. For small scales, a power-law behavior is expected between $Z_q(a)$ and a; that is, $Z_q(a) \sim a^{\tau(q)}$, with $\tau(q)$ an exponent which characterizes the scaling behavior at different scales. For positive q, the statistics reflect the scaling of large fluctuations and strong singularities, while for negative q, the statistics reflect small fluctuations and weak singularities. The exponent $\tau(q)$ is related to the Hurst exponent through the relationship $\tau(q) = qh - 1$, where $h = \mathrm{d}\tau(q)/\mathrm{d}q$. Note that, for monofractal signals, $\mathrm{d}\tau(q)/\mathrm{d}q = H$, with H a constant for the entire signal. The singularity spectrum $f(h)$ is obtained by means of the Legendre transform, given by $f(h) = q\mathrm{d}\tau(q)/\mathrm{d}q - \tau(q)$. We characterize the multifractality properties of signals based on $\Delta h = h_{\max} - h_{\min}$, which represents the width of the singularity spectrum, and h^*, which is the value that maximizes $f(h)$. When $h^* = 0.5$, we refer to an uncorrelated random walk, when $h^* > 0.5$ to a process dominated by fluctuations with positive long-range correlations, and when $h^* < 0.5$ to a process with antipersistent correlations.

4. Results

4.1. Monofractal analysis

First, we apply the FDM to cyclic heat release fluctuations obtained from simulations according to the model described in Section 2. Representative cases of heat release sequences are shown in Fig. 1. We show fluctuations for several values of ϕ within the range 0.5–1.1. A direct application of the FDM to the heat release sequences shown in Fig. 1 reveals that the scaling behavior is represented by exponents close to 2, which correspond to white noise fluctuations. However, the FDM becomes highly inaccurate for anticorrelated signals, especially for sequences with spectral exponent within the interval $-1 < \beta < 1$ [22,41]. For a more reliable application of the FDM to the heat release data, the sequence $Q(i)$ is first integrated to obtain the profile $Q_I(i) = \sum_{j=1}^{i}(Q_j - \bar{Q})$, with $\bar{Q}$ the mean value. In this way, the integrated signals lead to fractal dimensions within the vicinity of $D = 1.5$, where the FDM has been proved to estimate a stable scaling exponent [22,41,42]. For instance, a white noise sequence leads to a fractal dimension value of $D = 1.5$, and corresponds to the case where events are not correlated. For $D > 1.5$, the fluctuations resemble antipersistent behavior, whereas, for $D < 1.5$, the variations are described as persistent with long-range correlations. Fig. 2 shows representative cases of $\langle L(k)\rangle$ versus k for integrated heat release sequences and several values of the fuel ratio. We observe that, for high and low values of ϕ, the statistics follow a power-law behavior with an exponent slightly larger than $D = 1.5$ (see the next paragraph for a quantitative evaluation), indicating that the heat release values are close to uncorrelated variations with a weak antipersistence; that is, the heat release values tend to alternate. In contrast, for intermediate values of the fuel ratio, we identify two regimes separated by a crossover point.

To get a good estimation of D-values and the crossover point, we consider the following procedure: given the statistics of $\langle L(k)\rangle$, a sliding pointer along k is considered to perform linear regression fits to the values on the left and to the elements on the right. At each position of the pointer, we calculate the errors in the fits (e_l and e_r) and monitor the total error defined by $e_t = e_l + e_r$. We define two stable exponents (D_S and D_L) when e_t reaches its minimum value and the position of the crossover point is within the interval $10 \leq k \leq 500$. The results of this analysis are depicted in Fig. 3. We observe that, for intermediate values of ϕ, over short scales the fractal dimension is smaller than $D_S = 1.5$, whereas for large scales the exponent D_L is close to the white noise value. It is important to remark that, for both low and high fuel ratio values, the scaling exponent ($D \gtrsim 1.5$) is identified with a weak antipersistent behavior with anticorrelated fluctuations, whereas at intermediate values the scaling exponent for short scales is quite different (smaller) than the uncorrelated value $D = 1.5$, revealing that at small scales the fluctuations are correlated with a weak persistent behavior, in the sense that an increment of the heat release value is more likely to be followed by an increment, and the same occurs for decrements. Fig. 3 also shows how, around $\phi = 0.65$, D_S reaches a kind of minimum value. For this case, the crossover point which separates short and large regimes is located around $k^* \approx 20$ cycles. According to Heywood [43], engine performance measurements have showed that the engine stability limit evidenced by a minimum fuel consumption and onset of rapid increase in hydrocarbon emissions occurred at $\phi = 0.65$, just

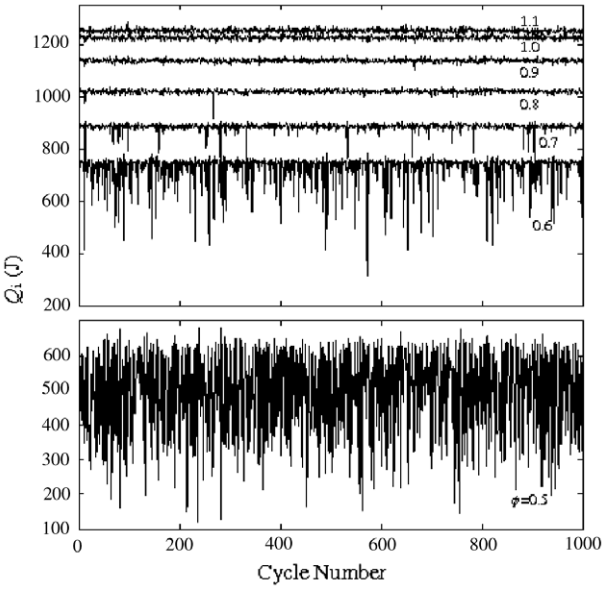

Fig. 1. Representative sequences of heat release fluctuations for several values of ϕ. We observe evident changes in the mean and standard deviation of the signals as ϕ decreases. For intermediate values of ϕ, we identify the presence of multiple outliers corresponding to low values of heat release.

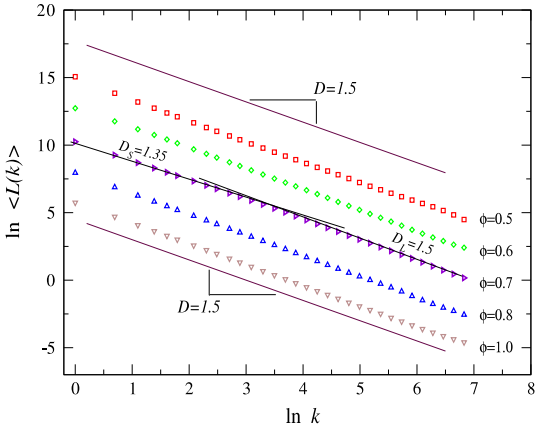

Fig. 2. Plot of $\ln\langle L(k)\rangle$ versus $\ln k$ of heat release sequences for several values of the fuel ratio ϕ.

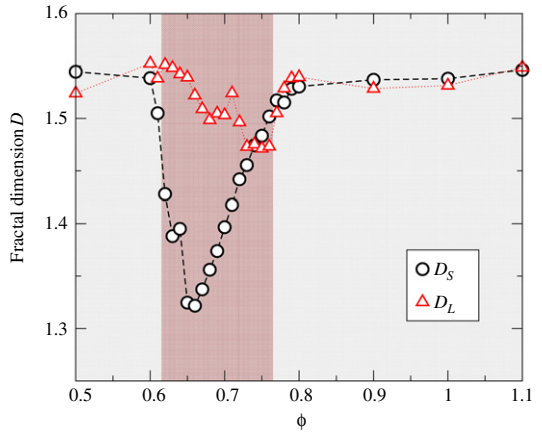

Fig. 3. Statistics of D_S and D_L for several values of the fuel ratio ϕ. For intermediate values of ϕ, two scaling regimes are identified, separated by a crossover point. For short scales we observed $D_S < 1.5$, whereas for large scales $D_L \approx 1.5$.

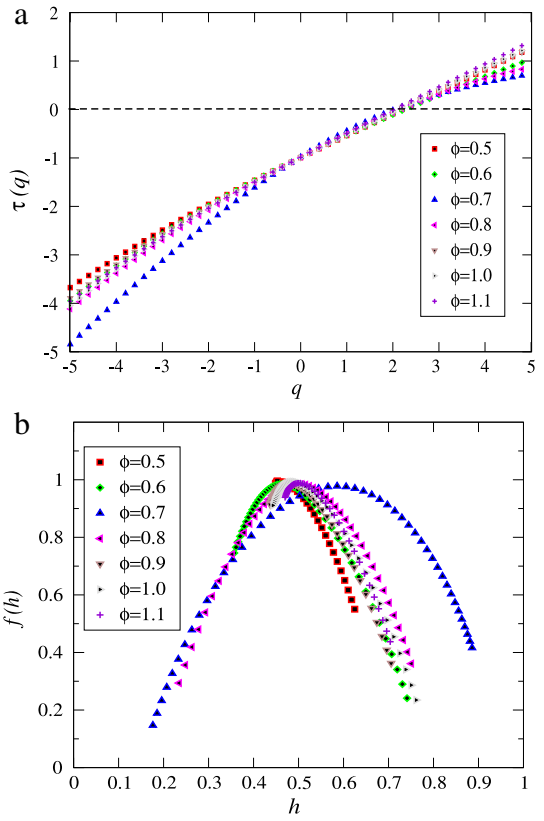

Fig. 4. Multifractal analysis of heat release variations. (a) Multifractal spectrum $\tau(q)$ for several values of ϕ. For intermediate values of ϕ, a nonlinear relationship is identified indicating multifractality. (b) Singularity spectrum $f(h)$ versus h for the cases shown in (a).

before the partial-burn limit where some slow-burning cycles occur but combustion is still complete in all cycles. That is, around $\phi \approx 0.65$ is the border between complete combustion cycles and partial burn until values of $\phi \approx 0.5$, where many misfires occur. Besides, around $\phi \approx 0.65$, the quasi-dimensional numerical model studied here produces combustion heat time series corresponding to a low-dimensionality dynamics [21], which represents deterministic behavior of CV, which according to Scholl and Russ [44] is a consequence of incomplete combustion. On the other hand, in Fig. 3 we observe that, for low and high values of ϕ, both D_S and D_L are equal to or bigger than 1.5, corresponding to dynamical regimes close to white noise of fluctuations with antipersistent behavior.

4.2. Multifractal analysis

To get further insight in the analysis of cyclic fluctuations, we apply the multifractal method to the integrated variations of heat release. Fig. 4(a) shows the behavior of $\tau(q)$ versus q for several values of ϕ from lean to stoichiometric conditions. We observe that, for intermediate values of the fuel ratio, a nonlinear behavior between $\tau(q)$ and q is identified, revealing multifractal properties of the signal. Fig. 4(b) shows that, for intermediate values of ϕ, the singularity spectrum is broad, confirming the multifractality of the signal. In contrast, for high and low fuel ratio values, an almost linear relationship between $\tau(q)$ and q is identified (Fig. 4(a)), which indicates a monofractal property, as can be seen in Fig. 4(b), where $f(h)$ is described over a narrow range of exponents h. The statistics of the singularity spectrum further reveal that, for intermediate values of ϕ, the local Hurst exponents cover a broad range related to multifractality (see Fig. 5(a)). Interestingly, we observe that the highest degree of multifractality is reached for values around $\phi \cong 0.68$. The statistics of the local exponent h^* which maximizes the singularity spectrum are summarized in Fig. 5(b). From this figure, it is clear that there is a transition for h^* from $h^* < 0.5$ to $h^* > 0.5$ as the fuel ratio varies from $\phi = 0.5$ to 0.65, and vice versa from $\phi = 0.78$ to 0.8, revealing that, for intermediate values of the fuel ratio, the fluctuations are dominated by a positive correlated behavior, whereas for high and low fuel ratio the dynamics can be described as processes with antipersistent variations. We also observe that the maximum value of h^* occurs when $\phi \approx 0.67$, which roughly corresponds to the value where the fluctuations reach the highest degree of multifractality (Fig. 4(b)). All these results are consistent with the results of the FDM analysis of the previous section.

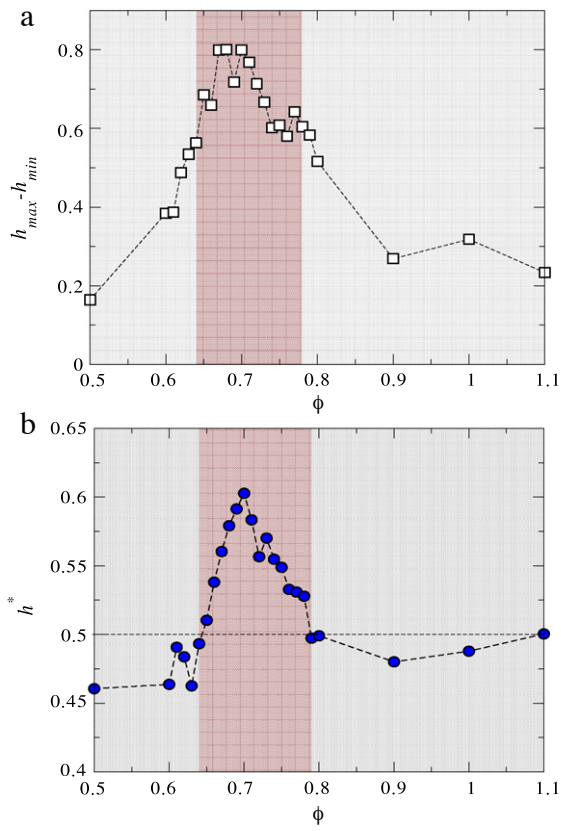

Fig. 5. (a) Width of the singularity spectrum $\Delta h = h_{\max} - h_{\min}$ versus ϕ. A broad spectrum represents a high degree of multifractality. (b) Statistics of h^* versus ϕ. For $h^* > 0.5$, the process is dominated by positive correlations, whereas, for $h^* < 0.5$, the process is described as anticorrelated. We observe that, for intermediate values of ϕ, the dominant dynamics can be described as positively correlated.

5. Discussion and conclusions

We have analyzed heat release sequences for different fuel ratio values. Our results show that there are important changes in the dynamical behavior as ϕ changes: particularly, transitions from a weak anticorrelated to a positive correlated behavior for short scales. In order to further evaluate the presence and origin of correlations in the signals, we repeated our calculations with surrogated sequences obtained from random permutations of the heat release values and from a phase randomization of the sequence. For the first case, the original sequence was randomly shuffled to destroy temporal correlations but preserving the distribution of events. For the second case, the surrogate set was constructed by a phase randomization of the original sequence. In this way, nonlinearities are eliminated, preserving the original power spectrum and changing the distribution. The phase randomization was performed after applying the FFT algorithm to the original time series to obtain the amplitudes. Then the surrogate set was obtained by applying the inverse FFT procedure [45,46]. Fig. 6 shows the fractal dimension results for shuffled and phase randomized data. For shuffled data, the values of D_S and D_L are close to the values of the original data (Fig. 3), while phase randomized data are characterized by a single fractal dimension with value close to $D = 1.5$, indicating an uncorrelated behavior even for intermediate values of the fuel ratio.

Multifractal analysis reveals that shuffled data are close to original series while phase randomized data exhibit a narrow spectrum close to a monofractal behavior (Fig. 7(a)). Fig. 7(b) shows the results of h^* versus ϕ, revealing that phase randomized data exhibit uncorrelated fluctuations with values around $h^* \approx 0.5$, while for shuffled data the dominant dynamics for intermediate values of the fuel ratio is quite similar to that observed in the original data (Fig. 5(b)). The results from shuffled and phase randomized sequences for intermediate fuel ratios suggest that phase correlations are important because when they were eliminated the fluctuations exhibited a monofractal behavior (narrow spectrum) with scaling exponents close to uncorrelated dynamics. We also remark on the fact that, for shuffled data, the scaling exponents are close to those observed in the original data, whereas phase randomization resulted in uncorrelated dynamics, suggesting that the observed correlation exponents for the original simulated data are mainly related to the distribution of events. More specifically, multifractality and correlated behavior could be associated to the characteristics of the probability density function; this is supported by the fact that the shuffled data show almost no changes in the scaling exponents with respect to the original data [47]. According to the statistics presented in previous studies for both experimental and simulated data [4,21], the kurtosis and skewness are quantities which dramatically increase for intermediate values of the fuel ratio. All

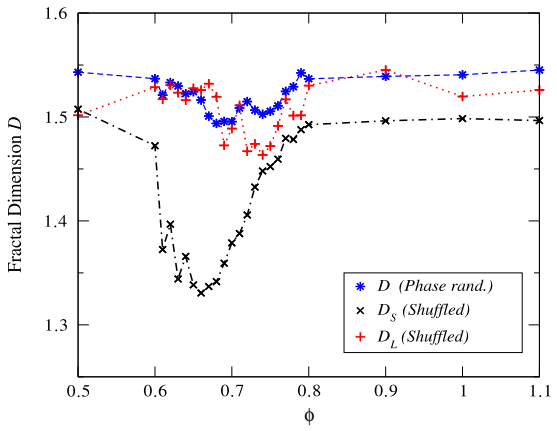

Fig. 6. Statistics of D_S and D_L for shuffled and phase randomized heat release sequences. Phase randomized data are described by one scaling exponent which is close to the white noise value, whereas shuffled data lead to values which are close to those from the original simulated data (Fig. 3).

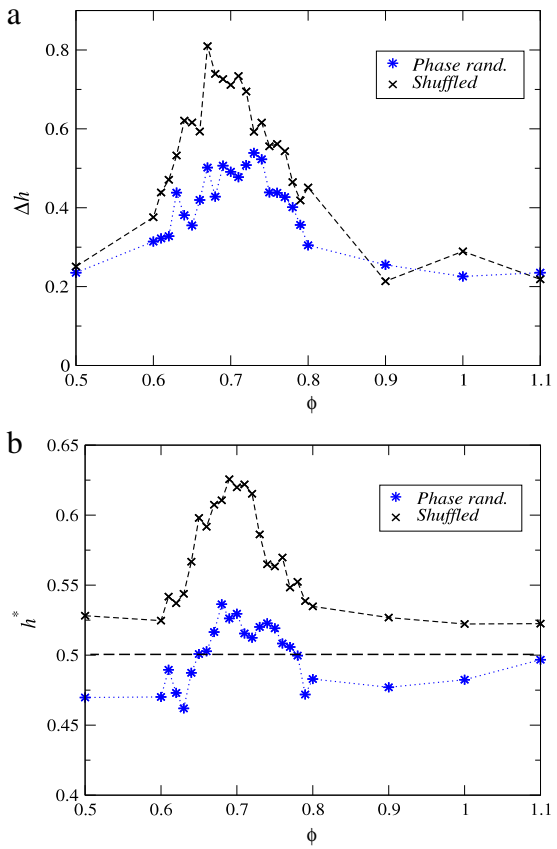

Fig. 7. Results of multifractal analysis for shuffled and phase randomized heat release sequences. (a) Width of the singularity spectrum $\Delta h = h_{\max} - h_{\min}$ versus ϕ. Phase randomized data are described by a narrow spectrum even for intermediate values of ϕ, indicating a low degree of multifractality. For shuffled data, the width of the spectrum is quite similar to that observed in the original data. (b) Dominant local Hurst exponent h^* versus ϕ. We observe that for phase randomized data the fluctuations are dominated by uncorrelated dynamics, whereas for shuffled data the dominant dynamics is similar to that observed in the original data (Fig. 5).

these results support the argument that, for intermediate values of ϕ, mainly around $\phi \approx 0.67$, a kind of dynamical transition occurs corresponding to the so-called engine stability limit, which according to Heywood is found around $\phi \approx 0.65$ [43]. This limit separates the regime where the combustion is still complete in all cycles and the regime of partial burn, which for very lean conditions leads to many misfiring events.

Acknowledgements

The authors acknowledge financial support from *Ministerio de Educación y Ciencia* of Spain under Grant FIS2006-03764 FEDER, and also from *Junta de Castilla y León* under Grant SA054A08. P.L.C.-R. acknowledges a pre-doctoral grant from Grupo Santander-Universidad de Salamanca. L.G.-V. and F.A.-B. thank COFAA-IPN, EDI-IPN and Conacyt (49128-26020), México.

References

[1] M.J. Moran, H.N. Shapiro, Fundamentals of Engineering Thermodynamics, John Wiley & Sons, 2007.
[2] C.S. Daw, M.B. Kennel, C.E.A. Finney, F.T. Connolly, Phys. Rev. E 57 (1998) 2811.
[3] T. Kaminski, M. Wendeker, K. Urbanowicz, G. Litak, Chaos 14 (2004) 461.
[4] A.K. Sen, G. Litak, C.E.A. Finney, C.S. Daw, R.M. Wagner, Appl. Energy 87 (2010) 1736.
[5] A.K. Sen, G. Litak, T. Kaminski, M. Wendeker, Chaos 18 (2008) 033115.
[6] G. Litak, T. Kaminski, R. Rusinek, J. Czarnigowski, M. Wendeker, Chaos Solitons Fractals 35 (2008) 578.
[7] N. Ozdor, M. Dulger, E. Sher, SAE (1994) Paper No. 940987.
[8] E. Abdi Aghdam, A.A. Burluka, T. Hattrell, K. Liu, G.W. Sheppard, J. Neumeister, N. Crundwell, SAE (2007) Paper No. 2007-01-0939.
[9] J.A. Rocha-Martínez, T.D. Navarrete-González, C.G. Pavía-Miller, A. Ramírez-Rojas, F. Angulo-Brown, Int. J. Ambient Energy 27 (2006) 181.
[10] G. Litak, T. Kaminski, J. Czarnigowski, A.K. Sen, M. Wendeker, Meccanica 44 (2009) 1.
[11] G. Litak, R. Taccani, R. Radu, K. Urbanowicz, J.A. Holyst, M. Wendeker, A. Giadrossi, Chaos Solitons Fractals 23 (2005) 1695.
[12] P.C. Ivanov, L. Amaral, A. Goldberger, S. Havlin, M. Rosenblum, Z. Stuzik, H. Stanley, Nature 399 (1999) 461.
[13] A. Goldberger, L. Amaral, J. Hausdorff, P.C. Ivanov, C.-K. Peng, H. Stanley, Proc. Natl. Acad. Sci. USA 99 (2002) 2466.
[14] M. Costa, A.L. Goldberger, C.-K. Peng, Phys. Rev. Lett. 89 (2002) 068102.
[15] L. Telesca, V. Lapenna, F. Vallianatos, Phys. Earth Planet. Inter. 131 (2002) 63.
[16] L. Telesca, V. Lapenna, M. Macchiato, Physica A 354 (2005) 629.
[17] L. Telesca, V. Lapenna, Tectonophysics 423 (2006) 115.
[18] L.-Y. He, S.-P. Chen, Physica A 389 (2010) 3218.
[19] M.-Y. Bai, H.-B. Zhu, Physica A 389 (2010) 1883.
[20] P.L. Curto-Risso, A. Medina, A. Calvo Hernández, J. Appl. Phys. 104 (2008) 094911.
[21] P.L. Curto-Risso, A. Medina, A. Calvo Hernández, L. Guzmán-Vargas, F. Angulo-Brown, (2010) (submitted for publication) arXiv:1005.5410.
[22] T. Higuchi, Physica D 46 (1990) 254.
[23] P.L. Curto-Risso, A. Medina, A. Calvo Hernández, J. Appl. Phys. 105 (2009) 094904.
[24] J.C. Keck, Proceedings of Nineteenth Symposium (International) on Combustion, The Combustion Institute, Pittsburgh, 1982, pp. 1451–1466.
[25] N.C. Blizard, J.C. Keck, SAE (1974) Paper No. 740191.
[26] G.P. Beretta, M. Rashidi, J.C. Keck, Combust. Flame 52 (1983) 217.
[27] J.B. Heywood, Internal Combustion Engine Fundamentals, McGraw-Hill, 1988, ISBN: 0-07-028637-x, pp. 402–406 (Chapter 9).
[28] O.L. Gülder, Tech. Rep. 841000, SAE, 1984.
[29] H. Bayraktar, O. Durgun, Energy Convers. Manage. 46 (2005) 2317.
[30] C.R. Ferguson, Internal Combustion Engines, John Wiley & Sons, 1986, p. 121 (Chapter 3).
[31] B.J. McBride, G. Sanford, Users Manual 1311, National Aeronautics and Space Administration, NASA, 1996. URL: http://www.grc.nasa.gov/WWW/CEAWeb/.
[32] G. Woschni, SAE (1967) Paper No. 670931.
[33] P.L. Curto-Risso, A. Medina, A. Calvo Hernández, Appl. Therm. Eng. (2010) (submitted for publication).
[34] C.K. Peng, S. Havlin, H.E. Stanley, A.L. Goldberger, Phys. Rev. Lett. 70 (1995) 1343.
[35] G. Rangarajan, M. Ding, Phys. Rev. E 61 (2000) 4991.
[36] T. Higuchi, Physica D 31 (1988) 277.
[37] J. Feder, Fractals, Plenum Press, New York, 1988.
[38] B.B. Mandelbrot, The Fractal Geometry of Nature, 2nd ed., Freeman, San Francisco, 1982
[39] J.F. Muzy, E. Bacry, A. Arneodo, Phys. Rev. Lett. 67 (1991) 3515.
[40] A.L. Goldberger, L.A.N. Amaral, L. Glass, J.M. Hausdorff, P.C. Ivanov, R.G. Mark, J.E. Mietus, G.B. Moody, C.-K. Peng, H.E. Stanley, Circulation 101 (2000) e215.
[41] G. Gálvez-Coyt, A. Munoz-Diosdado, J.L. del Río-Correa, F. Angulo-Brown, Fractals 18 (2009) 235.
[42] D.T. Schmitt, P.C. Ivanov, Am. J. Physiol. 293 (2007) R1923.
[43] J.B. Heywood, Internal Combustion Engine Fundamentals, McGraw-Hill, 1988, pp. 100–154 (Chapter 4).
[44] D. Scholl, S.G. Russ, SAE (1998) 980893.
[45] J. Theiler, S. Eubank, A. Longtin, B. Galdrikian, J.D. Farmer, Conference Proceedings on Interpretation of Time Series from Nonlinear Mechanical Systems, Elsevier North-Holland, Inc., New York, NY, USA, 1992, pp. 77–94.
[46] T. Schreiber, A. Schmitz, Physica D 142 (2000) 346.
[47] J.W. Kantelhardt, S.A. Zschiegner, E. Koscielny-Bunde, A. Bunde, S. Havlin, H.E. Stanley, Physica A 316 (2002) 87.